LAWRENCE
LIVERMORE
NATIONAL
LABORATORY

LLNL-PROC-674871

Ghost Fringe Removal Techniques Using Lissajous Data Presentation

D. J. Erskine, J. Eggert, P. Celliers, D. Hicks

July 20, 2015

APS Shock Cmprs. Cndsd. Matter
Tampa, FL, United States
June 14, 2015 through June 19, 2015

Disclaimer

LLNL-PROC-674871

Ghost Fringe Removal Techniques Using Lissajous Data Presentation

David Erskine[1,a)], Jon Eggert, Peter Celliers[1] and Damien Hicks[2]

[1]*L-487, Lawrence Livermore Nat. Lab., Livermore, CA 94550*
[2]*Center for Micro-Photonics, Swinburne Univ. Techn., Hawthorn, Victoria 3122, Australia*

[a)]Corresponding author: erskine1@llnl.gov

Abstract. Unwanted reflection of laser light from target windows can produce an additional component to the VISAR fringe record that can obscure and complicate the true signal. Accurately removing this so-called ghost component is essential for achieving high accuracy EOS measurements, especially when the true signal is only weakly reflected from the shock front. Independent of the choice of algorithm for processing the raw data into a complex fringe signal, we have found it beneficial to plot this signal as a Lissajous and seek the true center of this curve, since the ghost contribution is solved by a translation in the complex plane that recenters the Lissajous. For continuous velocity histories, we find that plotting the fringe visibility vs nonfringing intensity and optimizing linearity is a valuable tool for determining the proper ghost offsets. For discontinuous velocity histories, we have developed methods which relate the results of two VISARs having different velocity per fringe proportionalities to find the ghost offset.

July 29, 2015

INTRODUCTION

The VISAR velocity interferometer[1, 2, 3] is an important diagnostic for shock physics and equation of state (EOS) experiments, that measures the time history of Doppler shifted light reflected from shock or ramp loaded targets. The laser illumination often accesses the target through a window, rather than a free surface, to tamp the end of the target. Unwanted reflection of light from the target window, which might have an insufficient antireflection coating, can produce an additional zero velocity component to the VISAR interferogram, called a ghost fringe, that can obscure and complicate the true science signal. Accurately removing this ghost artifact is essential for achieving high accuracy EOS measurements, especially when the science signal is only weakly reflected from the shock front in some targets, such as in a normally transparent material barely at a pressure which creates a reflecting shock.

Figure 1(a) shows an example of a streak camera VISAR interferogram (data record) having a prominent ghost fringe artifact, and (b) with the artifact removed showing only the science component of the signal. The time is displayed horizontally and fringes splayed out vertically in phase. Time dependent Doppler velocity shifts produce proportional time dependent phase shifts $[\theta(t)]$, with a velocity per fringe (VPF) proportionality inversely dependent on a chosen interferometer delay, so that the fringe per velocity (FPV) increases with increasing delay. Panel (c) shows data taken simultaneous to (a) but with another VISAR with a smaller delay, so the phase shift for the same target velocity is smaller. The smaller science phase shift makes it more challenging to distinguish it from the stationary ghost. This is a motivation for accurately understanding how to best remove a ghost fringe.

For example, a popular method of distinguishing the ghost from science components is to take a 2d-Fourier transform of the interferogram, with the hope that the science and ghost components would make separate peaks in frequency space. The slope is related to the frequency manifested in the 2d-FFT. With the slope being shallow, there is the danger that the science and ghost peaks partially overlap, and thus deletion of the zero frequency peak and region around it would also inadvertently delete some of the frequencies of the science peak. While we find that the FFT zero frequency deletion method removes a majority of the ghost, it often does not do a perfect job.

We introduce a new graphically inspired method, “vector offset”, which we find intuitive and accurate. (We have previously developed analytical equations[4] relating net fringe visibility to ghost amount, and these complement the

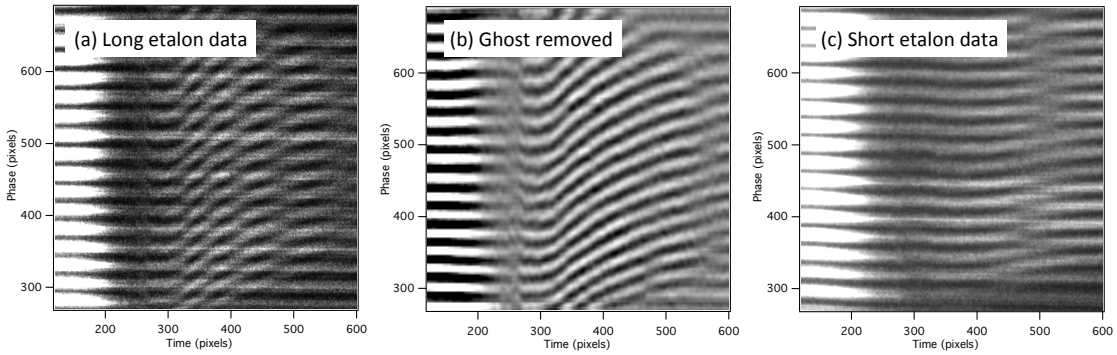

FIGURE 1. (a)(c) Example streak camera VISAR records having a prominent stationary artifact (ghost fringe) together with the moving science signal. The telltale "beats" in fringe visibility (magnitude) indicate presence of a ghost. These are most easily seen in the long etalon data (a) where the phase varies more strongly. The (b) shows (a) after ghost artifact is removed. The (c) shows the short etalon data measured simultaneous to the long etalon data (a), having proportionally smaller phase change vs time, so its ghost fringes are more similar in slope to the science fringes. This makes it more challenging to separate for the conventional method. Horizontal axis are pixels in time direction, vertical axis are y-pixels along streak camera slit direction which encode interferometer phase (and position across target). Omega shot s57519.

graphically inspired approach here.) Figure 2 shows a vector interpretation of what happens during ghost removal. The sinusoidal portion (the fringing portion) of the VISAR interferogram, i.e. apart from the nonfringing portion, can be expressed as a complex function $\mathbf{W}(t)$ whose real and imaginary parts represent the sine and cosine amplitudes of the sinusoidal shape for a column of the interferogram at a given time t. Equivalently, when $\mathbf{W}$ is expressed in polar coordinates, the magnitude and phase of $\mathbf{W}$ represents the fringe visibility and phase.

Various algorithms for converting fringes to $\mathbf{W}(t)$ (i.e. phase and magnitude) are popular, including an FFT method[5], a sine fit along a column, and push-pull treatment of four rows at 90 degrees[2, 6]. (The article Ref. 7 on line-imaging velocimetry, section on data reduction, is a good review.) A new algorithm that compensates for Y-variation of illumination and phase, called Speckle Adaptive, was used to process the streak VISAR data here, described by one of the authors [Erskine] in another contributed paper in this conference[8].) The ghost removal analysis described here can work with any algorithm that outputs both $\mathbf{W}(t)$ and the nonfringing intensity NF(t), and all algorithms can be made to output these. (The nonfringing intensity is the vertical offset in a sine fit, or the zero frequency component in a FFT output, or the sum of the four push-pull quadrature signals.)

The complex value of $\mathbf{W}$ can be represented by a vector in the complex plane. The angle of the vector (phase of the fringe) is proportional to the target Doppler velocity. Both the reflection from the stationary window and the moving shock interface generate fringes, which add vectorially. While the ghost vector remains at zero velocity, the science portion begins at zero velocity at t_0 and then evolves to other angles versus time. The initial angle θ_0 that corresponds to zero velocity is found from the data at t_0 or any time before the initial shock loading. Often this is already subtracted so that the ghost vector lies along the horizontal axis in many of the Figures.

The plotting of imag $\mathbf{W}$ vs real $\mathbf{W}$ is a Lissajous plot (Figure 2), and is a very useful means of presenting VISAR fringe data for a variety of reasons, not limited to ghost artifact, but including detecting other pathologies of the fringe to $\mathbf{W}(t)$ conversion. These tend to distort the path from a circular to a lopsided shape. The (b) shows that the science signal alone $W_{sci}(t)$ is a loop-like path centered at the origin. The presence of a ghost artifact W_{ghst} shifts the center of the loop by a vector offset, $\mathbf{W} = \mathbf{W}_{sci} + \mathbf{W}_{ghst}$.

Therefore one can remove the ghost artifact by shifting the $\mathbf{W}(t)$ by some amount $\mathbf{G}_{corr}$, ala $\mathbf{W} = \mathbf{W}_{sci} + \mathbf{W}_{ghst} - \mathbf{G}_{corr}$, searching until the resulting Lissajous is properly centered. We do not need to know the correction amount, it is sufficient just to center $\mathbf{W}$, then use this modified $\mathbf{W}$ to compute the velocity history.

Alternatively, one can use the FFT method to find and then delete all near zero frequency components of $\mathbf{W}(t) = \mathbf{W}_{sci}(t) + \mathbf{W}_{ghst}$. Since $\mathbf{W}_{ghst}$ is of zero frequency, it will certainly be removed, but the deletion process may also inadvertently remove some "good" near-zero frequency signals of $\mathbf{W}_{sci}(t)$. The presumption was that $\mathbf{W}_{sci}(t)$ does not have a large zero frequency component, and so it is not harmed, but we will show this is not a good presumption in many cases, especially for the short etalon VISAR.

The FFT method of finding the zero frequency is related to finding the average value $\langle \mathbf{W}(t) \rangle$. So we only need

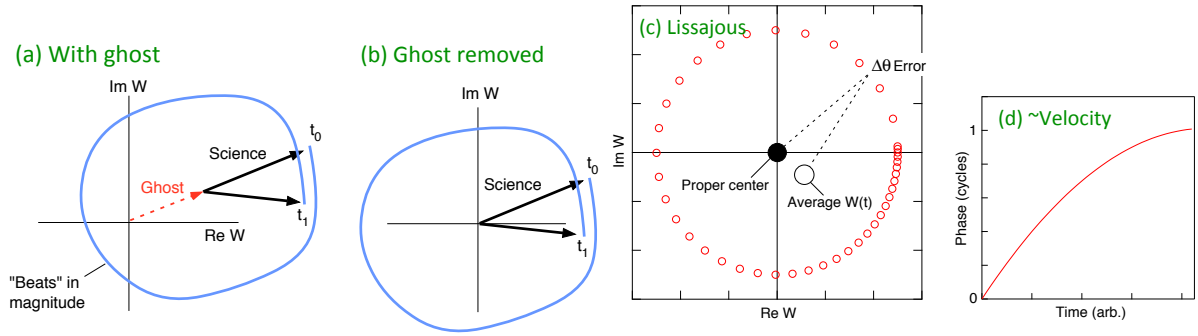

FIGURE 2. LEFT– How fringes of streak data appear when represented as a complex fringe signal $\mathbf{W}(t)$ and plotted as a Lissajous path (light blue) in the complex plane, where $\Im\mathbf{W}$ is plotted vs $\Re\mathbf{W}$ over some time region t_0 to t_1. Each of two velocity components (ghost, science) corresponds to a vector, which sum. The angle of the vector is proportional to Doppler velocity, divided by the velocity per fringe proportionality VPF. The length of the vector is the fringe's sinusoidal magnitude, which is proportional to the amount of coherent light reflected from the target. The ghost artifact vector (red) remains at zero velocity, while the science vector changes angle (and less strongly, magnitude) with time. It makes a loop-like structure when it changes phase continuously by more than one cycle, such as during the decay behind a shock front. Removal of the ghost contribution translates the science portion so that it is recentered around the origin. RIGHT– Example of how the average value of $\mathbf{W}(t)$, i.e. the Fourier-computed center of the Lissajous path (c), can be nonzero if the target velocity, shown as change in Doppler induced phase shift (d), has nonuniform acceleration. If the angular extent of the total phase change is not an integer number of cycles, that can also shift the average of $\mathbf{W}(t)$.

to show that $\langle \mathbf{W}_{sci}(t) \rangle$ is significant to show that there is a problem. For the long etalon VISAR where the Lissajous make many loops, than perhaps it is a reasonable approximation to say that the average value is small. However, for the short etalon which creates fewer loops, the $\langle \mathbf{W}_{sci}(t) \rangle$ can be significant. This can happen either when the total phase change not an integer number of cycles, or when the slope of velocity vs time is nonlinear (Figure 2[c][d]), or when the reflected intensity varies (Figure 3).

Theory

Some equations describing the formation of fringes in an interferometer from the light of two surfaces (shock and and stationary window) include

$$I(t,y) = I_{bb}(t) + Lsr(t)R(t)\{1 + \gamma \cos 2\pi[\theta(t) + \theta_0 + y]\} + Lsr(t)G\{1 + \gamma \cos 2\pi[\theta_0 + y]\} \quad (1)$$

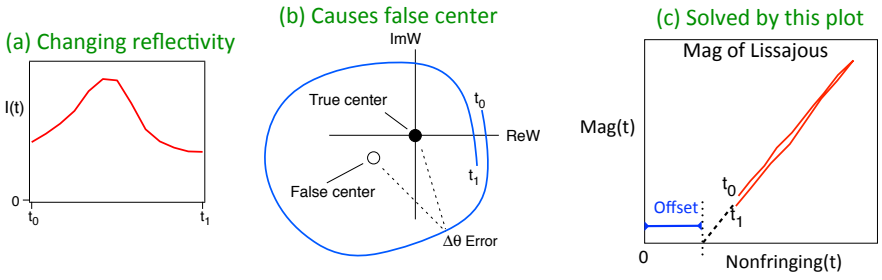

FIGURE 3. Example of how the average value of $\mathbf{W}(t)$ can shift due to variable reflectivity that varies over a similar time that the phase changes about one cycle. This creates an apparent center not at the origin. The true center can be located at the origin by plotting in panel (c) the magnitude of the Lissajous ($|\mathbf{W}(t)|$) vs nonfringing intensity, and translating the Lissajous by adding a constant complex constant to $\mathbf{W}$ until the plot (c) has minimized its deviation from a line or spot). The line will be horizontally offset from the origin due to the nonfringing component of the ghost reflection, plus any target incandescence or detector bias.

$$\mathbf{W}(t) = \{[I(t,0) - I(t,180)] + i[I(t,90) - I(t,270)]\}/2 \quad (2)$$
$$NF(t) = \{I(t,0) + I(t,90) + I(t,180) + I(t,270)\}/4 \quad (3)$$

$$\mathbf{W} = \mathbf{W}_{sci} + \mathbf{W}_{ghst} - \mathbf{G}_{corr} \quad (4)$$
$$NF = NF_{sci} + NF_{ghst} \quad (5)$$

$$W_{sci} = Lsr(t)R(t)\gamma\, e^{i2\pi[\theta(t)+\theta_0]} \quad (6)$$
$$W_{ghst} = Lsr(t)G\gamma\, e^{i2\pi[\theta_0]} \quad (7)$$

$$Mag\ of\ \mathbf{W} = |\gamma Lsr(t)R(t)e^{i2\pi[\theta(t)+\theta_0]} + \gamma Lsr(t)Ge^{i2\pi[\theta_0]} - \mathbf{G}_{corr}| \quad (8)$$
$$Mag\ of\ \mathbf{W}_{sci} = \gamma Lsr(t)\, R(t) \quad (9)$$
$$NF = [I_{bb}(t) + Lsr(t)G] + Lsr(t)R(t) \equiv NF_{Hoffset} + Lsr(t)R(t) \quad (10)$$

The I_{bb} is any target incandescence or detector bias, and Lsr is laser illumination. The G and R are the ghost-creating window and shocked interface reflectivities. The $\theta(t)$ and θ_0 are science fringe history and time zero phase offset. The y is a unit of phase proportional to the position along the streak camera slit, and changes units with context. For example, I(t,90) means intensity along the interferogram row at the y position that produces 90 degrees of interferometer output phase. The $\mathbf{W}$ is the complex fringing output, and NF the nonfringing intensity. The subscripts "sci" and "ghst" represent science and ghost components. The $\mathbf{G}_{corr}$ is the vector offset that we apply to center the Lissajous of $\mathbf{W}$.

The γ is the instrument visibility and is ideally unity and decreases with misalignment of the optics. It can also decrease due to the velocity texture of the reflecting surface. (If the reflecting surface has a variety of Doppler shifts producing a variety of phase shifts, these can wash each other out if their standard deviation is a quarter cycle or larger.)

Mag vs Inten Plot Indicates Lissajous Centration

Figure 3(c) Shows a type of plot we find extremely useful for determining the absence of various distortions in the fringing data including the presence of ghost offset. It is the magnitude of the Lissajous $|\mathbf{W}(t)|$ versus the nonfringing intensity $NF(t)$. In the absence of all distortions that can affect the fringing signal (including distortions caused by the algorithm converting the interferogram to $\mathbf{W}(t)$), the Mag vs NF plot should be linear, since increasing the intensity of light reaching the interferometer will increase both the nonfringing and fringing terms.

By translating the $\mathbf{W}(t)$ data to maximize the linearity of the Mag vs NF plot, which is to say we minimize the standard deviation of the data about a line or point, we find the shape of $\mathbf{W}(t)$ without the ghost.

Why Does This Work?

In Eq. 9 the magnitude of the science fringes after we have successfully removed the ghost is $\gamma Lsr(t)R(t)$, proportional to the 2nd term of the $NF(t)$ of Eq. 10. Hence plotting Mag vs NF and removing the ghost by adjusting $\mathbf{G}_{corr}$ will make a line of slope γ, provided that the horizontal offset $NF_{Hoffset} \equiv [I_{bb}(t) + Lsr(t)G]$ is not changing with time significantly, which is an approximation.

This seems to work in practice for many shots, even though in reality the laser intensity may vary 10 to 30% during the record. The key reason is that while $Lsr(t)$ may vary, *it varies much slower than* $R(t)$. So at each place that $R(t)$ changes rapidly, a *locally* linear feature is made, (and the $NF_{Hoffset}$ for it may be slightly different for each feature because $Lsr(t)$ wanders).

We have success correcting some shots with a series (about four) of ghost vectors of different lengths over different time periods. This is a crude way of modeling a changing $Lsr(t)$. In principle, a more comprehensive analysis that models the laser intensity history with a continuous function would produce even more accurate results.

Example on Recent Data

Figure 4(a) shows raw streak VISAR interferogram having a weak ghost, one not apparent just by casually looking at this image but only after inspecting the Lissajous (d). There, and especially in the Mag vs NF plot (e), it becomes

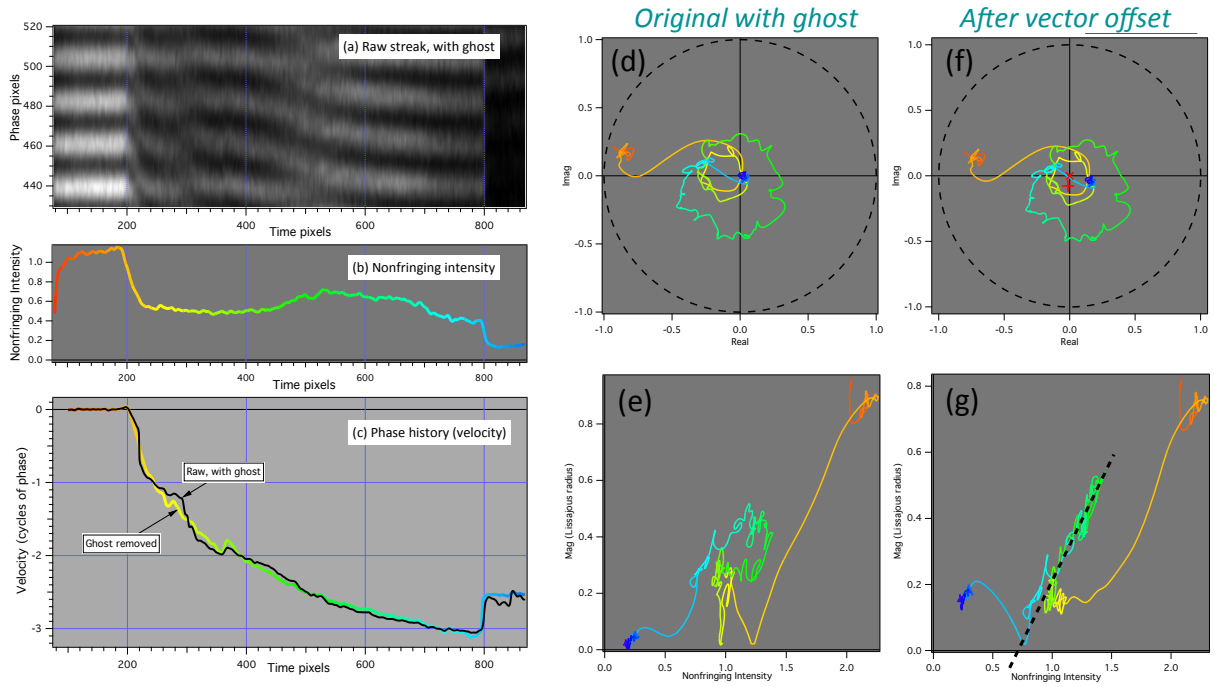

FIGURE 4. LEFT– (a) Streak record of Omega shot 75265 on cubic BN– data obtained by Amy Lazicki. Casual visual inspection of (a) does not suggest obvious ghost presence, but it is there, as shown by lack of centration in Lissajous. Nonfringing intensity (b) and phase vs time (c, black curve) were obtained from (a) for the rows Y = 450 to 496 (2 fringes). Colored phase vs time curve is after ghost was removed by our vector offset technique– note that erroneous wiggles (phase errors of order 0.25 cycle) in the black curve are now absent. Color of curve corresponds to time. RIGHT– The ghost can be detected by a Lissajous (d)(f), but even more precisely by a Mag vs NF plot (e)(g). The (d)(e) is raw data $\mathbf{W}(t)$ of (a). The (f)(g) is that data offset by complex constant (0.115,-0.03), which was chosen to minimize the deviation of the data relative to a line in the Mag vs Inten plot (g). Red "X" in (f) indicates the proper center of the Lissajous as determined by our technique, now located at the origin because we have translated the data to do that. Red "+" indicates the average of this offset Lissajous, over time range 200 to 800 pixels. This would be the proper center determined by the conventional technique, and note it is different from our result "X". This would produce an phase error as much as about 30 degrees for the yellow time period, judged by the angle subtended by a point on the yellow portion of the curve to the "X" and to the "+".

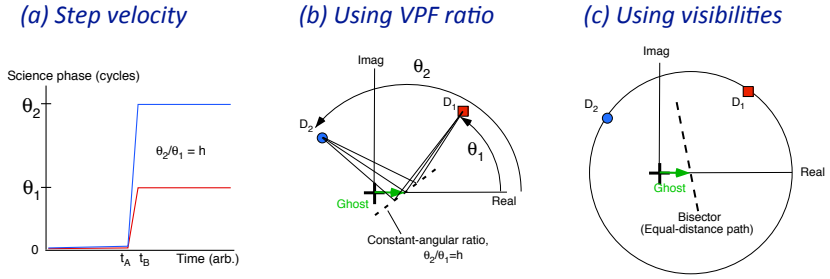

FIGURE 5. (a) A discontinuous jump in velocity (phase) from zero velocity, as in a single shock, presents a different kind of analysis challenge from the continuous phase history type discussed in previous Figures. It is common practice to simultaneously observe the target with two VISARs having velocity per fringe proportionality (VPF) that are different (often in ratio between 1 to 3, i.e. 2.3x). This produces a phase change from zero in a ratio $h \equiv \theta_2/\theta_1$. In this Figure zero phase is along the horizontal axis, hence the ghost vector (green) also points along this axis, but with an unknown length. (b) Where the loci of points (dashes) that satisfy a constant angular ratio intersects the horizontal axis tells the length of the ghost vector. (c) If the relative fringe magnitude is assumed to be consistent between the two VISAR systems (i.e. change from its zero velocity magnitude by the same fractional amount), then ghost vector should lie along the bisector (i.e. equal-distance) between shocked complex fringe values D_1 and D_2.

obvious that the yellow time portion loop of the Lissajous is not centered. Figure 4(c) black curve is the velocity (with the ghost) and shows more wiggles than what one expects for a smoothly decaying pressure wave.

Then we begin translating the Lissajous (d)(f) while observing the result on the Mag vs NF plot (e)(g). The gross direction to translate is down and to the left, suggested by the desire to center the yellow time portion. This portion, due to its small radius, is the most sensitive to translation. The Mag vs NT plot (g) is used to fine-tune the translation, as the green time portion forms up into a nice line and the yellow portion into a tight ball.

The translation which produces the tightest grouping is (0.115,-0.03). Now that we have corrected W, a velocity is extracted from its phase. This is plotted in Figure 4(c) as colored curve.

Mag vs NF Also Useful As Canary

This method of optimizing Mag vs NF intensity linearity is generically useful for minimizing many other distortions of the fringing data, not only ghost offset, but also including distortions created by poor math assumptions in the algorithm converted the interferogram to $\mathbf{W}(t)$, such as having unanticipated nonlinear phase vs Y, or uncorrected laser illumination variation vs Y. Each type of pathology produces a different kind of distortion, which deviates the Lissajous from circularity and therefore makes ripples in the Mag vs NF plot. These distortions are described further in reference [9] and corrected with the adjustable gains of their Eq. 2-5 and Eq. 10-11. Thus this Mag vs Intensity plot (c) is extremely useful as a canary in the coal mine. If a nicely linear behavior is observed, one can be confident that all these potential distortions are absent and the analysis cannot be improved further.

Strategies for Discontinuous Jumps

We have developed strategies for computing ghost contributions for velocity profiles that have a discontinuous jump and no portion with a ramp or continuous decaying portion. The lack of continuous portion prevent loop-like Lissajous, making it less obvious by inspection where the proper center would be. Figure 5(b) shows methods inspired by geometry and the assumption that two different VISARs observing the same target are used, having a ratio $h = VPF_1/VPF_2$ in their velocity per fringe proportionalities, so that the angular position is related by a ratio $h = \theta_2/\theta_1$. Figure 5(c) shows a graphical method assuming the relative fringe visibilities behave the same in the two VISAR systems, so one knows that the ghost vector must lie on the bisector between the two step positions D_1 and D_2.

ACKNOWLEDGMENTS

Thanks to Amy Lazicki for Omega data she obtained. Prepared by LLNL under Contract DE-AC52-07NA27344.

REFERENCES

[1] L. Barker and K. Schuler, J. Appl. Phys. **45**, 3692–3693 (1974).
[2] W. Hemsing, Rev. Sci. Instr. **50**, 73–78 (1979).
[3] D. Dolan, Sandia National Laboratory Tech. Rep. **SAND2006-1950** (2006).
[4] P. M. Celliers, J. H. Eggert, D. G. Hicks, *et al.*, http://link.aps.org/supplemental/10.1103/PhysRevLett.104.184503 Phys. Rev. Lett. **104** May (2010).
[5] M. Takeda, H. Ina, and S. Kobayashi, Journal of the Optical Society of America (1917-1983) **72**, p. 156 January (1982).
[6] W. M. Trott, M. D. Knudson, L. C. Chhabildas, and J. R. Asay, "Measurements of spatially resolved velocity variations in shock compressed heterogeneous materials using a line-imaging velocity interferometer," in *American Institute of Physics Conference Series*, American Institute of Physics Conference Series, Vol. 505 (2000), pp. 993–998.
[7] P. M. Celliers, D. K. Bradley, G. W. Collins, D. G. Hicks, T. R. Boehly, and W. J. Armstrong, Rev. Sci. Instr. **75**, 4916–4929 November (2004).
[8] D. J. Erskine, "Speckle-adaptive VISAR Fringe Analysis Technique", AIP Conf. Series, 19th APS Topical Conf. Shock Cmprssn. Cndsd. Matter, Tampa, FL, June 14-19, 2015, paper H3.00004.
[9] D. J. Erskine, R. F. Smith, C. A. Bolme, P. M. Celliers, and G. W. Collins, Rev. Sci. Instr. **83**, p. 043116 (2012).